IJE TRANSACTIONS B: Applications Vol. 39, No. 05, (May 2026) 1226-1237

International Journal of Engineering

Journal Homepage: www.ije.ir

Ensuring Vibration Strength of Mainline Pumping Unit Systems Using Digital Prototypes

I. N. Budilov[a], S. N. Tyulyandin*[b]

[a] Department of Mechanics, Empress Catherine II Saint Petersburg Mining University, Saint Petersburg, Russia
[b] Department of Transport and Storage Oil and Gas, Empress Catherine II Saint Petersburg Mining University, Saint Petersburg, Russia

PAPER INFO

Paper history:
Received 05 May 2025
Received in revised form 21 June 2025
Accepted 14 July 2025

Keywords:
Computational Modeling
Digital Prototype
Finite Element Method
Mainline Pumping Unit
Multiphysics Models
Vibration-compensation System

ABSTRACT

The relevance of this research stems from the necessity to enhance existing vibration-compensation systems for reducing vibrational loads on power units of mainline pumping units (MPUs). Algorithms and computational results of the spatial vibration state of the vibration-compensation system (VCS) for MPUs under various operational regimes are presented. Mathematical and spatial finite-element models, as well as versatile digital prototypes of the VCS, have been developed. The novelty of the findings lies in the developed digital prototype of the MPU, which offers broad capabilities for accounting for design-technological factors, accommodates diverse operational regimes, and exhibits high precision and computational efficiency. The practical significance of the work is that the developed simulation methodology based on digital prototypes of the MPU VCS enables the analysis of vibrational impacts from electric motors, pumps, and load-bearing frames. Comprehensive computational studies of the stress-strain state of the VCS frame were performed, and the system's natural frequencies during operation were evaluated. The objective of this work is to study the behavior of the pumping unit when replacing elastomeric supports in the compensation system with hydrofilm dampers. An indisputable advantage of the developed digital model is its foundation for a universal methodology to assess the effectiveness of vibration compensators in the MPU VCS. A unique digital prototype of the MPU was developed considering the engineered VCS. The feasibility of using a finite-element-based digital prototype for evaluating vibrational loading on MPUs is substantiated. Numerical experiments using the MPU's digital twin established that implementing hydrofilm dampers in the VCS reduces peak dynamic stresses by 18%. Values of axial and resultant displacements of the MPU using hydrofilm and elastomeric dampers in the VCS were obtained, measuring 11.1 mm and 10.0 mm, respectively.

***doi**: 10.5829/ije.2026.39.05b.15*

Graphical Abstract

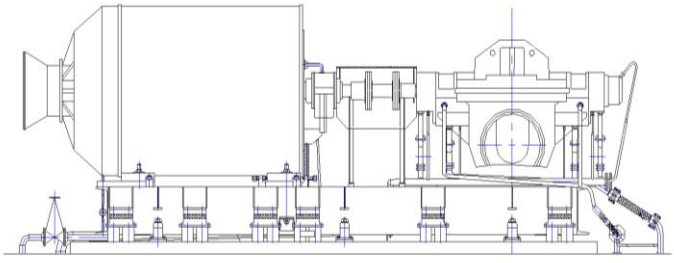

Resonant frequencies of the rigidly mounted MPU

Frequency, Hz						
f_1	f_2	f_3	f_4	f_5	f_6	f_7
38,2	52,2	55,3	59,1	62,4	65,7	66,8

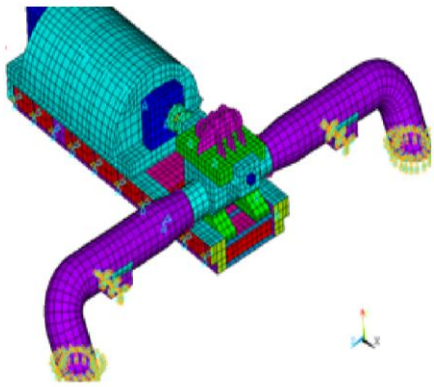

* Corresponding Author Email: s235105@stud.spmi.ru (S. N. Tyulyandin)

Please cite this article as: Budilov IN, Tyulyandin SN. Ensuring Vibration Strength of Mainline Pumping Unit Systems Using Digital Prototypes. International Journal of Engineering, Transactions B: Applications. 2026;39(05):1226-37.

1. INTRODUCTION

Mainline pumping units (MPUs) are widely used in oil and gas transportation systems to maintain pressure during fluid transfer and are integral components of oil pumping stations (OPS).

VCSs for MPUs often include bellows compensators to reduce static and dynamic loads transmitted from pipelines to the pump.

However, computational and experimental analyses (1) demonstrate limited compensation efficiency due to the pressure-dependent stiffness of bellows compensators, which becomes comparable to the stiffness of pipeline bends during MPU operation.

The generally accepted global practice in the design and manufacturing of mainline pumping units (MPUs) involves the expert evaluation of technical solutions based on digital prototypes (2, 3). In the field of improving the design of vibration compensation systems (VCS), notable works are known (4, 5). By utilizing digital prototypes and relying on the fundamental laws of continuum mechanics (CM) embedded within them, as well as through the application of modern computational methods (6) it becomes possible to track trends in load increases when changing the operating parameters of VCS.

Digital prototypes also facilitate process optimization by isolating random factors inherent in real-world production and operation.

MPUs must maintain operational integrity under standard loads from connected pipelines, as per regulatory code NP-068-95[1]

Natural frequency calculations are mandatory for vibration strength verification (7-9), complying with SNiP 2.05.06-85 (10), GOST 32388 (11), and other standards (12-15), ensuring pipeline system reliability and safety (16-18) while accounting for gas distribution failure statistics (19, 20). MPU design per PNAE G-7-002-86 requires static strength, brittle fracture resistance, and vibration strength analyses (21). Studies (22-24) address pipeline crack propagation and fracture toughness assessment.

The implementation of novel approaches, particularly during initial design stages—specifically through the use of fuzzy Bayesian belief networks (FBBNs) (25)- enables significant risk reduction in addressing systemic challenges across project lifecycle phases. Machine learning further ensures high operational efficiency during preliminary prototype development (26).

This work validates the feasibility of equipping MPUs with vibration-compensation systems and selects optimal damper types. Stress-strain states and vibration levels were calculated for the NM 7000–210/STDP–6300–2BUKhL4/10000 MPU under static (weight, temperature, pressure) and dynamic (rotor unbalance) loads.

Four foundation mounting configurations were analyzed: rigid supports vs. dampers (AMP-1700, A-2000, AGP-2.1).

VCS Design Description. The external view of the NM 7000–210 MPU is shown in Figure 1.

The primary load-bearing components of the VCS include: the load-bearing frame, elastomeric dampers, a flexible coupling and a horizontal centrifugal pump with a double-suction impeller. The MPU is driven by an asynchronous STDP-6300 electric motor with a power output of up to 10 kW (25).

Vibrations in the MPU system arise from dynamic interactions between the pump-motor assembly and the load-bearing frame, which are subsequently transmitted to the foundation (26, 27). The pump and electric motor form a coupled dynamic system, generating significant vibrational loads (28, 29).

Since the MPU incorporates structural components with heterogeneous stiffness, these assemblies experience uneven dynamic loading. Consequently, the service life of the MPU is primarily determined by operational modes, pump inlet pressure, and the structural integrity of its flow path components (30, 31). The unit is also subjected to electromagnetic and hydrodynamic forces.

Frequent transitions between operational regimes—from nominal operation to start/stop cycles—coupled with prolonged transient-state operation, induce significant dynamic stress in load-bearing assemblies, adversely affecting the MPU's overall operational reliability.

Notably, the annual number of MPU starts can exceed 300, resulting in substantial dynamic loading intensity that further compromises operational durability (32).

A distinctive feature of the VCS is its incorporation of reactive supports equipped with elastomeric dampers. The primary objective in designing the VCS is to mitigate

Figure 1. The external view of the NM 7000–210 MPU/ STDP- 6300

[1] NP-068-95, Federal norms and rules in the field of atomic energy use «Pipeline fittings for nuclear power plants. General technical requirements».

dynamic loads acting on the MPU's load-bearing components.

2. 1. Problem Statement Despite the high operational efficiency of VCS in industrial applications, their drawback lies in the use of angular rubber-cord or straight-through compensators[1]. Current practice widely adopts hydrofilm dampers without compensators. Based on numerical modeling results of vibration load fields for both damped and rigidly mounted MPUs, recommendations are provided for installing MPUs on hydrofilm dampers.

Consider a VCS comprising: inlet pipes: 820×12 mm, weight per linear meter (oil-filled): 666.67 kg; outlet bend: Ø820 mm, mass (oil-filled): 678 kg.

The adjustable vibration-damping pipeline support consists of a steel plate with connecting and reinforcing elements, fitted with three elastomeric dampers (APM-1700) as shown in Figure 2.

2. 2. Spectral Analysis Equations In oil and gas field mechanics, the finite element method (FEM) (33), implemented in modern computational platforms, has gained widespread adoption[2].

TABLE 1. Characteristics of APM-1700 Dampers

Rated load, kgf	P_Y	**2000,0**
Static stiffness, kN/m	K_{xi}	410,0
	K_{zi}	330,0
	K_{yi}	5400,0
Dynamic stiffness, kN/m	K_{xi}	637,0
	K_{zi}	588,0
	K_{yi}	6020,0
Allowable vertical deformation, mm		32,0
Allowable horizontal deformation, mm		18,2

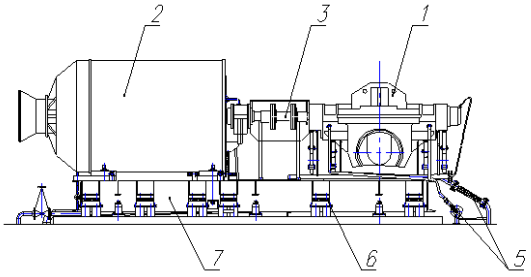

Figure 2. MPU NM 7000–210 MPU/ STDP-6300-2
1. Pump, 2. Electric motor, 3. UKM coupling, 4. MKS compensator-vibration dampers, 5. Flexible connections of auxiliary pipelines, 6. Elastomeric damping supports, 7. Reinforced unit frame; 8. Reactive supports for pipelines

The governing equation for evaluating undamped oscillations using spectral analysis can be expressed as follows (34-36):

$$[M]\{u"\}+[C]\{u'\}+[K]\{u\}=\{F\} \quad (1)$$

where [M]; [C], [K] - mass, damping, and stiffness matrices;

{u"},{u'},{u} - nodal acceleration, velocity, and displacement vectors.

The time-dependent force vector {F} is expressed as:

$$\{F\}=\{F^{nd}\}+s\{F^{s}\} \quad (2)$$

where: $\{F^{nd}\},\{F^{s}\}$ - load vectors; s - scaling coefficient.

The load vector $\{F^{s}\}$ is computed during modal analysis.

Introducing the substitution,

$$\{u\}=\sum_{i=1}^{n}\{\varphi_i\}y_i \quad (3)$$

into the system's equation of motion yields the governing equation:

$$[M]\sum_{i=1}^{n}\{\varphi_i\}y_i''+[C]\sum_{i=1}^{n}\{\varphi_i\}y_i'+[K]\sum_{i=1}^{n}\{\varphi_i\}y_i=\{F\} \quad (4)$$

where: $\{\varphi_i\}$ - i-th mode shape; n - number of modes; y_i;- modal coordinates.

Multiplying by $\{\varphi_j\}^{T}$, we derive the final equation:

$$\{\varphi_j\}^{T}[M]\sum_{i=1}^{n}\{\varphi_i\}y_i''+\{\varphi_j\}^{T}[C]\sum_{i=1}^{n}\{\varphi_i\}y_i'+ +\{\varphi_j\}^{T}[K]\sum_{i=1}^{n}\{\varphi_i\}y_i=\{\varphi_j\}^{T}\{F\} \quad (5)$$

or equivalently:

$$\{\varphi_j\}^{T}[C]\{\varphi_j\}=2\xi_j\sqrt{K_jM_j}\left(\frac{1}{\sqrt{M_j}}\right)^{2}=2\xi_j\omega_j \quad (6)$$

Introducing the notation

$$f_j=\{\phi_j\}^{T}\{F\} \quad (7)$$

The equation of motion becomes:

$$y_j''+2\omega_j\xi_jy_j'+\omega_j^{2}y_j=f_j \quad (8)$$

[1] Gumerov A.G., Gumerov R.S, Akberdin A.M. Diagnostics of oil pumping station equipment. M.: OOO «Nedra-Biznestsentr», 2003, 347 p.

[2] Finite element method in problems of oil and gas field mechanics. N. Alikin, I.E. Litvin, S.M. Shcherbakov, V.P. Borodavkin. M.: Nedra, 1992, 288 p.

2. 3. Description of Finite Element Model The digital prototype of the MPU, shown in Figure 3, includes the following components: the unit frame, the STDP-6300-2BUKhL4/10000 electric motor, the NM 7000–210 pump, the shaft assembly with a coupling, the inlet pipeline section, and the outlet pipeline section.

To assess the influence of the frame damper stiffness characteristics on the stress-strain state (SSS) of the MPU, three damped mounting configurations were analyzed: mounting on elastomeric dampers (APM-1700), mounting on elastomeric dampers (A-2000), and mounting on hydrofilm dampers (AGP-2.1)[1].

Simplifications in the model involve replacing mounting dampers with rod elements represented as spring-type elastic elements (COMBINE14) in three directions, accounting for the stiffness of actual dampers specified in Table 3. The model employed rigid contacts between connecting nodes of structural elements using "surface-to-surface" and "point-to-surface" types, with slippage of contact elements disregarded.

The finite element model (FEM) of the MPU incorporating boundary conditions is illustrated in Figure 4.

FEM Constraints: A distinctive feature of the FEM is the assignment of reduced density for various structural components. The mass of the inlet/outlet pipelines was calculated considering the contained fluid product, the motor mass corresponded to its simplified model representation, and the same approach was applied to the pump. The element size was selected based on the smallest constructible mesh dimension. The final FEM comprised 800,000 hexahedral elements, balancing analytical precision and computational efficiency.

Thermal stresses and subsequent total stresses in the pipes were derived via the superposition principle. Incremental calculations summed mechanical and thermal deformations using the formula:

$$\Delta\varepsilon^0 = \varepsilon^e + \varepsilon^T \quad (9)$$

where ε^e - elastic deformation increment, and $\Delta\varepsilon^T=\alpha\times\Delta T$ - increment of components accounting for thermal deformations, where α is the coefficient of linear thermal expansion.

2. 4. Calculation of Stress-Strain State of Nm 7000–210/STDP–6300–2 Unit The objective of this computational experiment is to perform a computational assessment of the stress-strain state (SSS) of the NM 7000–210/STDP–6300 MPU. Two installation configurations of the unit frame on the PS foundation were analyzed: mounting on rigid supports or on dampers, with pipelines resting on an adjustable vibration-damping support. This support consists of a steel plate with connecting and reinforcing elements, equipped with three elastomeric APM–1700 dampers.

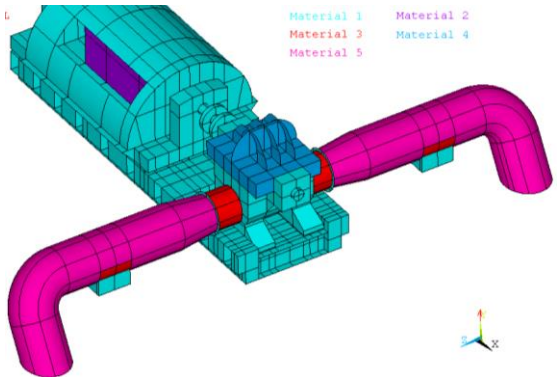

Figure 3. Solid-state model of MPU

The SSS evaluation of the MPU was conducted under the following loads: gravitational force (37), starting torque M_{st}=45410 N/m, temperature differential $\Delta t=20^0$C, inlet pipeline pressure p_1=2,8 MPa, and outlet pipeline pressure p_2=4,8 MPa. The SSS and vibration analysis for both installation configurations were performed using the finite element method (FEM) based on a digital platform (38).

2. 5. Description of Digital Prototype The FEM mathematical model employed five material types, whose properties are listed in Table 2. All materials corresponded to Grade 20 structural steel, with variations only in reduced density assignments to match the weight of individual components. The table also specifies their applications.

Material Group 1 corresponds to standard steel properties. For Groups 2–5, adjusted density values were assigned to ensure equivalence between the mathematical model's mass and the actual structural mass. Material Group 1 exhibits standard steel properties. Groups 2–5 feature reduced density values determined by equating

TABLE 2. Material Characteristics

№	E, Pa	ν	ρ, kg/m³	α·10⁵	Application
1	2,06·10¹¹	0,3	7850	1,1	Unit frame, shaft assembly
2	2,06·10¹¹	0,3	35500	1,1	Electric motor
3	2,06·10¹¹	0,3	15700	1,1	Pump, pipeline
4	2,06·10¹¹	0,3	12200	1,1	Pump
5	2,06·10¹¹	0,3	21700	1,1	Pipeline

[1] EIMA.304242.015 TU. Technical conditions. Metal plate shock absorbers of AMP type. Tekhnicheskie usloviya, Severodvinsk, PO «SevmaSH», 1996, 60 p.

the model's mass with the actual structural mass. Pipeline material corresponded to Grade 20 steel ([σ]=147,0 MPa, σ_B=410,0 MPa; σ_T=234,0 MPa), while the support frame material matched Grade 09G2S steel ([σ]=196,0 MPa, σ_B=500,0 MPa; σ_T=350,0 MPa).

The general configuration of the finite element model (digital prototype) of the MPU with boundary conditions is shown in Figure 4.

The finite element model includes components such as the unit frame, electric motor, shaft drive, coupling, pump, and pipeline. Shell-type finite elements were used for mesh generation, with displacement constraints applied as boundary conditions. A key constraint involves interactions between volumetric Solid 185 and shell-type SHELL63 elements with incompatible degrees of freedom. This limitation is resolved using next-generation SolSH 190 volumetric elements that maintain compatibility with shell elements (39).

The characteristics of the COMBINE14 elastic elements in terms of axial stiffness are provided in Tables 3 and 4.

3. RESULTS OF CALCULATIONS

The stress-strain state (SSS) of the rigidly mounted mainline pumping unit (MPU) was calculated under the following loads: gravitational force (g = 9,807 m/s^2 gravitational acceleration); starting torque M_{st} = 45,41 kN·m; temperature differential Δt = 20^{0}C; inlet pipeline pressure p_1 = 2,8 MPa; and outlet pipeline pressure p_2 = 4,8 MPa.

The SSS assessment under gravitational load was performed using static analysis in ANSYS/WORKBENCH 2019 R3. Calculations were performed on the workstation (processor: Intel i7-10920, memory: DDR4 64 GB, graphics processing unit (GPU): GeForce RTX 3070 Ti 12 GB, storage: Samsung SSD 2 TB). The total computation time was 4 hours. The general

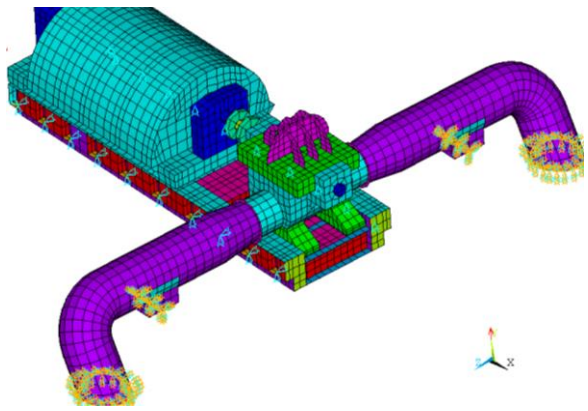

Figure 4. Mathematical model of the MPU accounting for boundary conditions

TABLE 3. Static characteristics of elastic elements

Designation	Static stiffness, N/m		
	AMP-1700	A–2000	AGP-2.1
K_X	0,41·10^6	1,47·10^6	0,91·10^6
K_Z	0,33·10^6	0,44·10^6	0,56·10^6
K_Y	5,40·10^6	2,16·10^6	1,98·10^6

TABLE 4. Dynamic characteristics of elastic elements

Designation	Dynamic stiffness, N/m		
	AMP-1700	A–2000	AGP-2.1
$\boldsymbol{K_X}$	0,64·10^6	1,96·10^6	1,35·10^6
$\boldsymbol{K_Z}$	0,59·10^6	0,84·10^6	0,95·10^6
$\boldsymbol{K_Y}$	6,02·10^6	2,84·10^6	2,10·10^6

view of the MPU mathematical model with boundary conditions and applied loads is shown in Figure 4. The SSS results are graphically presented as contour plots in Figures 5 to 8.

The von Mises criterion (40-43) was adopted as the basis for strength assessment. Stress distributions according to the von Mises criterion σ_{von} in the inlet pipeline and outlet pipelines are presented as contour bands and shown in Figure 8.

The maximum stress, σ_{max}=25,2 MPa, was observed at the central rigid support locations.

The SSS under combined operational loads was analyzed using an engineering analysis system (49, 50). The boundary conditions are illustrated in Figure 4.

Calculations in Figures 5a and 5b depict the loading scheme for the starting torque and pressure distribution in the pipeline and pump, respectively.

Figures 5a and 5b show the deformation pattern of the MPU with contour lines of resultant (Figure 5a) and vertical (Figure 5b) displacements. Dashed lines represent the undeformed state. Maximum displacements were calculated as follows: resultant displacement W_{max} = 0,0765·10^{-3} m; vertical displacement UY_{min} = – 0,0761·10^{-3} m.

Results in Figures 6 to 8 display contour plots of resultant, longitudinal, vertical, and lateral displacements. Extreme displacement values are: resultant: W_{max} = 1,72·10^{-3} m (Figure 5a); longitudinal: U_{Xmin} = – 1,437·10^{-3} м, U_{Xmax} = 1,422·10^{-3} m (Figure 5b); vertical: U_{Ymin} = – 0,250·10^{-3} m, U_{Ymax}=1,285·10^{-3} m (Figure 5b); lateral: U_{Zmin} = – 1,214·10^{-3} m, U_{Zmax} = 1,093·10^{-3} m.

Structural strength was evaluated using the Mises criterion. Figure 8 shows the Mises stress distribution across the MPU and its components. Maximum stresses were: outlet pipeline: σ_{out} = 285 MPa; Inlet pipeline:

σ_{inl} = 234,0 MPa; pump casing: σ_{pump} = 101,0 MPa; MPU frame: σ_{frame} = 25,5 MPa.

Thus, it has been established that the maximum stresses in the MPU occur at the outlet pipeline bend. This high-stress zone exhibits a localized character.

Forced vibration results for the rigidly mounted MPU are shown in Figures 9 to 14, including: -Frequency response of bearing and pipeline vibration displacements (Figures 9 and 10);

Vibration displacements at the motor bearing near the coupling and at the field-side motor bearing (Figure 10);

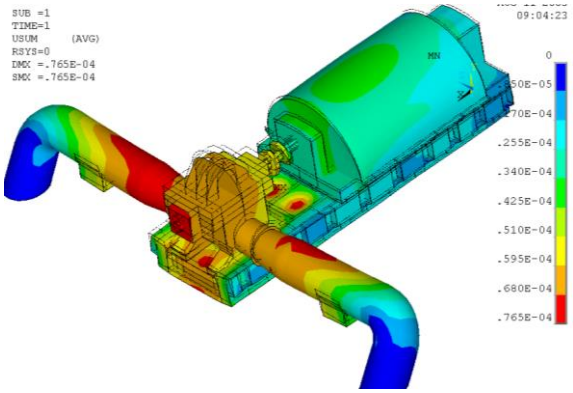

(a)

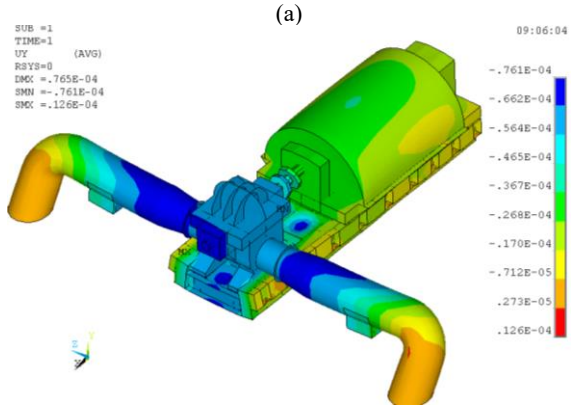

(b)

Figure 5. Resultant displacements (a) (m) and vertical displacements (b) (m) of the MPU

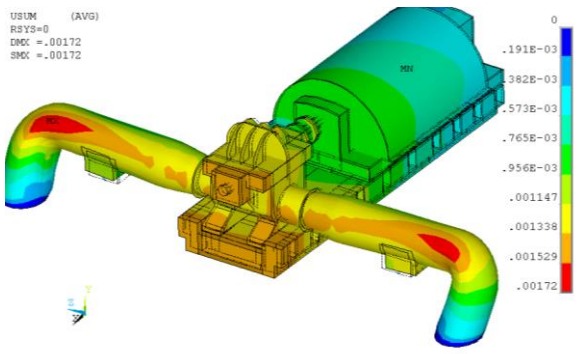

(a)

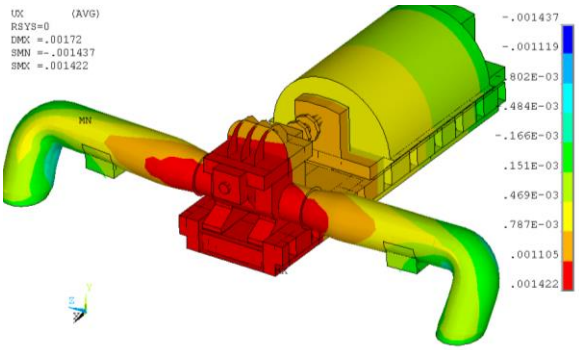

(b)

Figure 6. Total and longitudinal displacements of MPU (m)

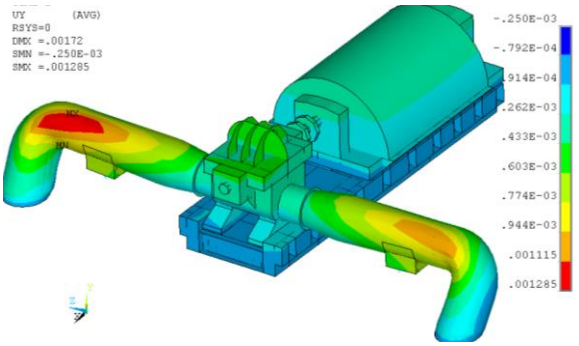

(a)

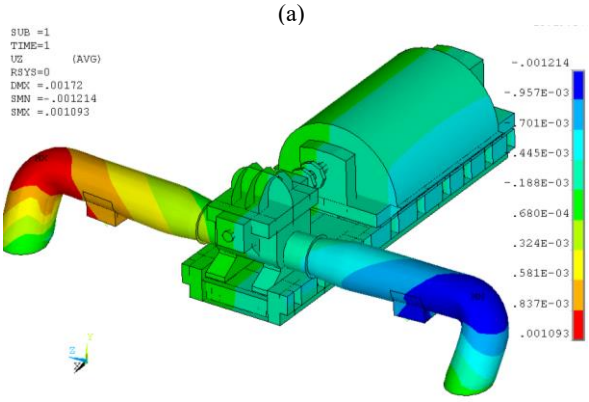

(b)

Figure 7. Vertical (a) and lateral (b) displacements of the MPU (m)

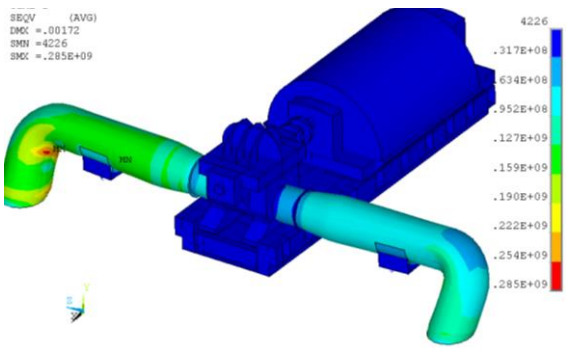

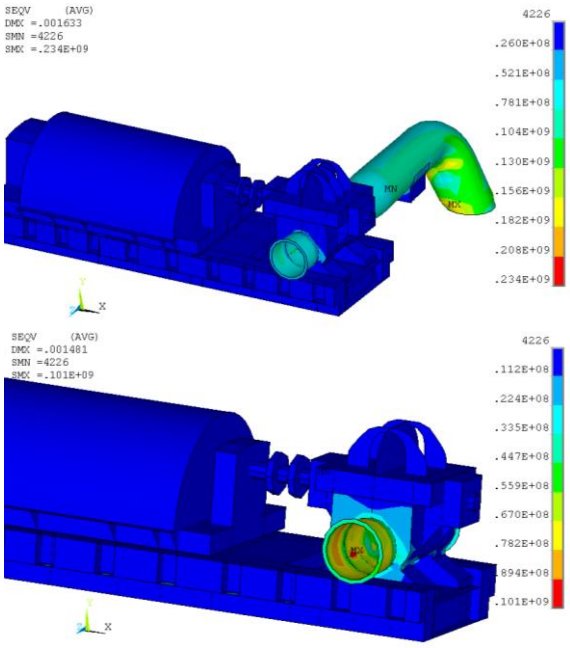

Figure 8. Equivalent stresses in the MPU inlet pipeline (Pa)

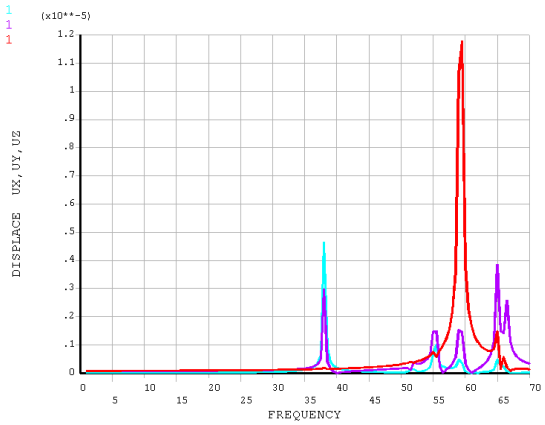

(a)

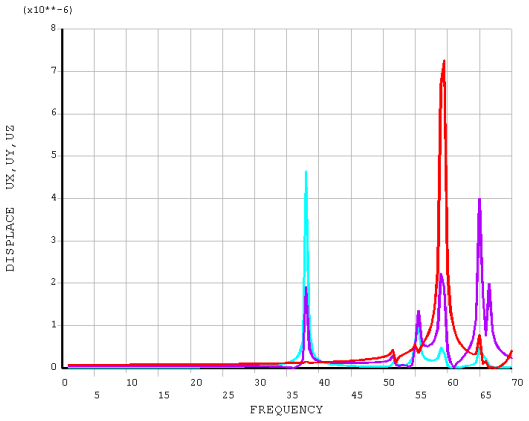

(b)

Figure 9. Vibration displacements of the non-damped MPU at the field-side pump bearing (a) and at the pump bearing near the coupling (b)

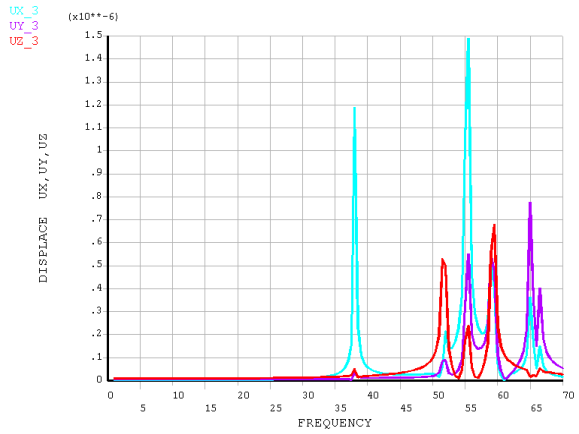

(a)

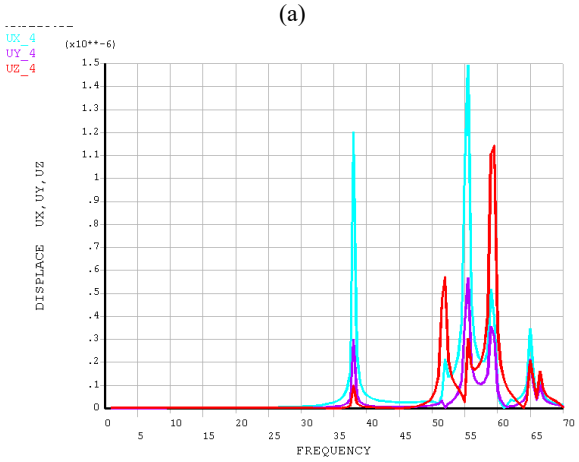

(b)

Figure 10. Vibration displacements at the motor bearing near the coupling (a) and at the field-side motor bearing (b) of the non-damped MPU

Vibration displacements at the outlet and inlet pipelines (Figure 11) and vibration displacements under the field-side motor bearing and motor bearing near the coupling (Figure 12);

The vibration responses of the non-damped MPU at points beneath the pump bearing are shown in Figure 13., and forced vibration mode shapes at resonant frequencies (Figure 14).

The calculated resonant frequencies of the rigidly mounted MPU are presented in Table 5. As evident from the data in Table 5, the first seven resonant frequencies of forced vibrations for the non-damped MPU nearly coincide with its natural frequencies (considering the frequency increment used in the calculations).

Of particular note is the presence of a dense cluster of intense resonances near the rotational frequency of the steady-state regime, as well as a resonance at 38 Hz. When passing through this frequency during startup, the accelerating rotor system of the unit (with a rotational speed of 2280 rpm) generates significant centrifugal excitation forces.

4. DISCUSSION OF RESULTS

Analysis of the digital prototype results revealed that the maximum stresses from static loads occur at the outlet pipeline bend, reaching 285.0 MPa for the non-damped MPU and 289.0 MPa for the damped MPU. Resultant pipeline displacements were 1.72 mm for the non-damped configuration, 2.67 mm for MPUs on AMP-1700 dampers, 2.29 mm for A-2000 dampers, and 2.49 mm for AGP-2.1 dampers.

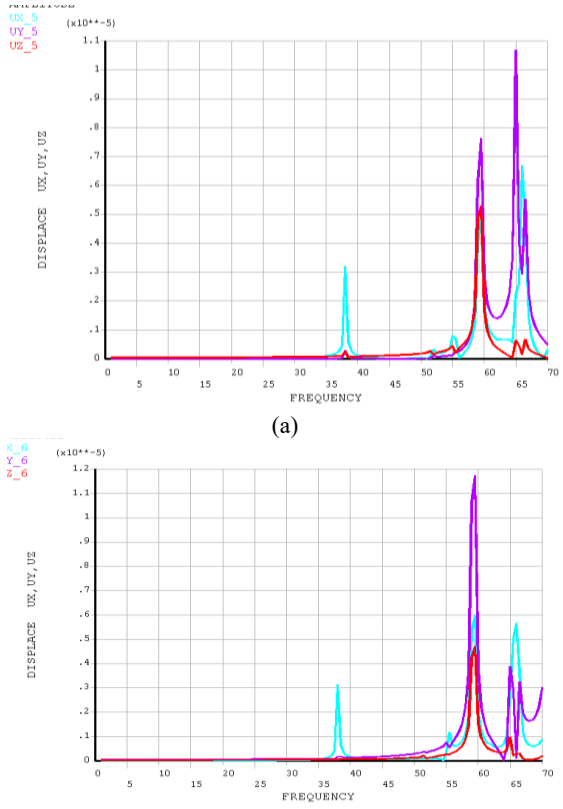

(a)

(b)

Figure 11. Vibration displacements at the outlet pipeline (a) and inlet pipeline (b) of the non-damped MPU

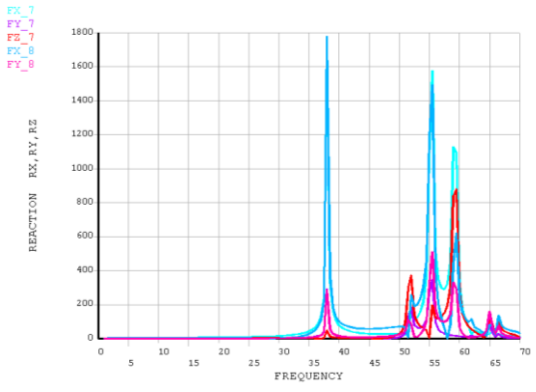

(a)

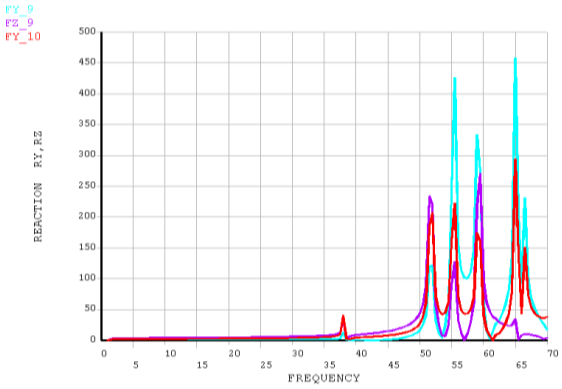

(b)

Figure 12. Vibration responses at points under the field-side motor bearing and under the motor bearing near the coupling of the non-damped MPU

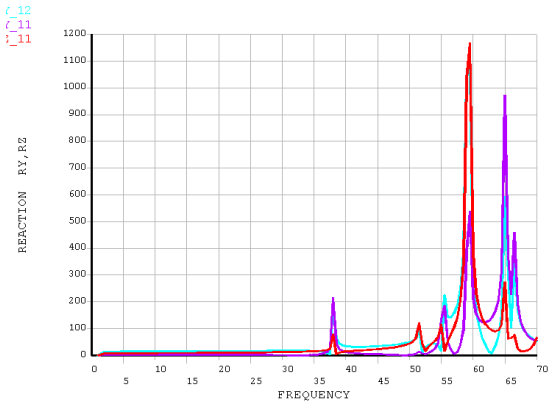

(a)

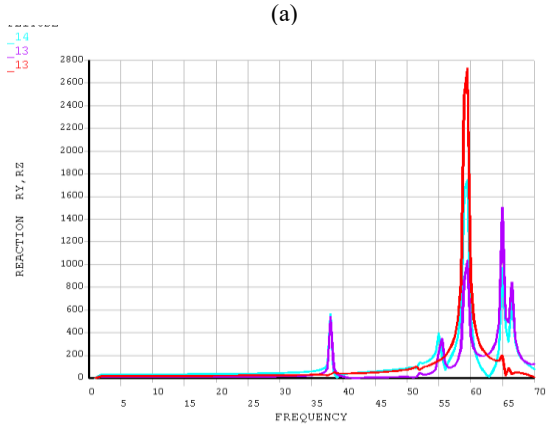

(b)

Figure 13. Vibration responses of the non-damped MPU at points under the pump bearing]

Under steady-state operation at the rotational frequency, the pump displacement was 8.0×10^{-6} m for the non-damped MPU, 6.0×10^{-6} m for MPUs on elastomeric AMP-1700 or A-2000 dampers, and 5.0×10^{-6} m for MPUs on AGP-2.5 hydrofilm dampers. Maximum stresses at the pump-pipe connection were 4.0 MPa for

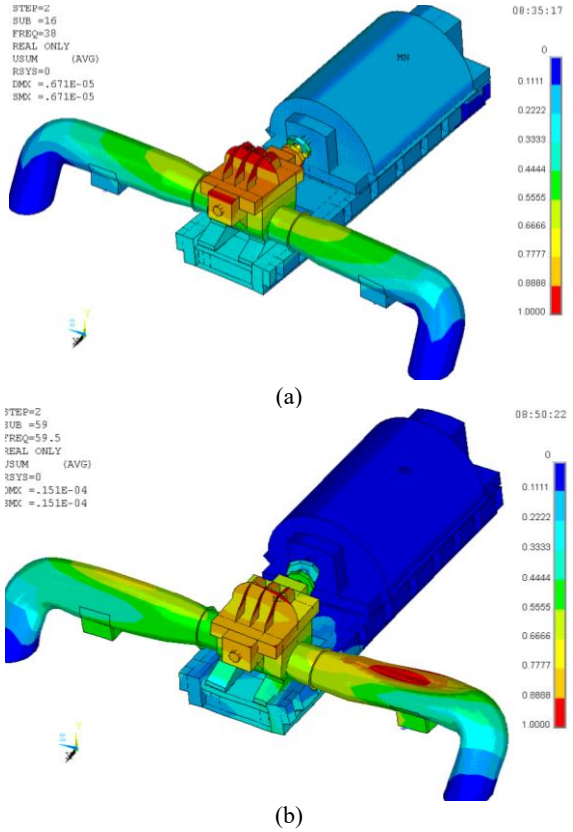

Figure 13. Forced vibration mode shapes of the non-damped MPU at 38 Hz (a) and 59.5 Hz (b)

TABLE 5. Dynamic characteristics of elastic elements

Frequency, Hz						
f_1	f_2	f_3	f_4	f_5	f_6	f_7
38,2	52,2	55,3	59,1	62,4	65,7	66,8

both non-damped and damped configurations, and 3.0 MPa for the damped configuration.

Vibration velocity amplitudes at the rotational frequency under steady-state conditions were: 2.66 mm/s for the non-damped MPU; 2.04 mm/s for MPUs on elastomeric AMP-1700/A-2000 dampers; 1.57 mm/s for MPUs on hydrofilm dampers.

The maximum levels of forced pump vibrations during startup were also obtained and analyzed. Thus, for the non-damped MPU, the maximum forced vibration levels of the pump amount to $8{,}0\cdot10^{-5}$ m with a pipe stress of 16.0 MPa at the pump-pipe connection area; for the MPU on elastomeric dampers – $5{,}0\cdot10^{-5}$ m with a pipe stress of 9.0 MPa at the pump-pipe connection area; and for the MPU on hydrofilm dampers – $4{,}0\cdot10^{-5}$ m with a pipe stress of 6.0 MPa at the pump-pipe connection area.

The maximum amplitude of forced vibration velocity during startup for the non-damped MPU is 19.20 mm/s, for the MPU on elastomeric dampers – 11.30 mm/s, and for the MPU on hydrofilm dampers – 9.01 mm/s.

The vibrational and dynamic characteristics of the non-damped MPU, obtained through computational analysis, show good agreement with experimental data. This also confirms the reliability of the computational results for the damped MPU.

Thus, based on the data obtained in this study, it can be concluded that the numerical experiments confirm the effectiveness of hydrofilm dampers within the VCS, as they reduce the overall vibrational loading on the MPU by 18.5%.

Experimental research documented in the field (7-9) and measurements conducted on operational units corroborate the findings of this numerical study.

The obtained data on the assessment and reduction of vibrational stress using hydrofilm compensators are explained by their design features and hysteresis loop characteristics under cyclic loading conditions.

The key strength of this work lies in the first-time development of a digital prototype and computational methodology for the vibration-compensation system of compressor stations. This approach enables the investigation of numerous design parameters and non-standard operational modes affecting vibrational stress in compressor stations, constituting the core advantage of this digital experiment over established methodologies.

5. CONCLUSIONS

The results of the calculations and experiments demonstrated the following:

1. Equipping the unit with dampers shifts its primary resonances to the low-frequency range, which significantly increases inertial resistance to transient processes and excitation forces, shifts resonances to regions of relatively low centrifugal excitation forces generated by the accelerating rotor system, and consequently reduces vibration amplitudes at resonant frequencies during startup.

2. The maximum stresses in the MPU pipeline occur at the bend due to static loads, are virtually independent of damping, and reach 280.0 MPa. The wall thickness of the bend was assumed equal to the pipeline wall thickness.

3. The maximum stresses from dynamic loads in the MPU pipeline occur at the pump connection point. Under steady-state operation at the rotational frequency, these stresses are also independent of damping.

4. Maximum stresses and vibration velocity amplitudes in the MPU pipeline caused by dynamic startup loads are lower in units with hydrofilm dampers

compared to elastomeric dampers, and significantly lower than in non-damped units.

5. Frequency responses of the damped MPU exhibit a resonance at 51.5 Hz, dangerously close to the operational rotational frequency. This resonance is inherent to the frame design and independent of damper type.

7. Maximum resultant displacements of the MPU near the field-side motor bearing were recorded as 10.3 mm for A-2000 dampers and 11.1 mm for AGP-2.1 dampers.

8. The developed universal digital prototype of the mainline pumping unit with piping systems and vibration-compensation system, along with the novel methodology for forced vibration calculation, enables:

- investigation of transient operational modes of the MPU;
- accounting for thermal conditions, pipeline pressures, and other factors affecting system vibration strength;
- future optimization of the load-bearing frame design to reduce mass-dimensional parameters while maintaining vibration strength reliability.

Author contributions:

Budilov Igor Nikolaevich, Dr. Sci. (Tech), Prof. of the Department of Mechanics, Empress Catherine II Saint Petersburg Mining University – research concept and design;

Tyulyandin Sergey Nikolaevich postgraduate student of the Department of Transport and Storage of Oil and Gas, Empress Catherine II Saint Petersburg Mining University – data collection, processing, statistical analysis, text drafting, and editing.

6. REFERENCES

1. Tokarev A, Zotov A, Valeev A. The application of passive vibroprotective systems having power characteristics with hysteresis loops of rectangular shape for the main pumping units. Procedia Engineering. 2017;176:118-27. 10.1016/j.proeng.2017.02.279
2. Sukhorukov A, Koryagin N, Eroshkin SY, Kovkov D, editors. Statistical modeling of the process of generating analog information in the problems of the digital economy. 2017 Tenth International Conference Management of Large-Scale System Development (MLSD); 2017: IEEE. 10.1109/MLSD.2017.8109691
3. Cherepovitsyn AE, Tretyakov NA. Development of a new assessment system for the applicability of digital projects in the oil and gas sector. Записки Горного института. 2023(262 (eng)):628-42.
4. Mukherjee S. A theoretical study and 3D modeling of nonlinear passive vibration isolator. International journal of Applied and Advanced Scientific Research (IJAASR). 2017;2(2). 10.5281/zenodo.996576
5. Werner U. Active vibration control for rotating machines with current-controlled electrodynamic actuators and velocity feedback of the machine feet based on a generalized mathematical formulation. Control Theory and Technology. 2025;23(1):1-27. 10.1007/s11768-024-00230-w
6. Fomichev P, Fomicheva E, editors. Optimization problems of the characteristics of vibroprotective systems of a new type. IOP Conference Series: Earth and Environmental Science; 2019: IOP Publishing. 10.1088/1755-1315/272/2/022102
7. Li Y, Li J, Li W, Du H. A state-of-the-art review on magnetorheological elastomer devices. Smart materials and structures. 2014;23(12):123001. 10.1088/0964-1726/23/12/123001
8. Anvar V, Alexey Z, Artem T. Study of application of vibration isolators with quasi-zero stiffness for reducing dynamics loads on the foundation. Procedia Engineering. 2017;176:137-43. 10.1016/j.proeng.2017.02.281
9. Zotov A, Tokarev A. A Dynamic Vibration Absorber with Adjustable Stiffness. Journal of Machinery Manufacture and Reliability. 2023;52(6):525-31. 10.1134/S1052618823050175
10. Tokarev A, Usmanova A, Godovskiy D, editors. Conditions for the Occurrence of Resonant Oscillations of Vertical Booster Pumping Units. IOP Conference Series: Earth and Environmental Science; 2022: IOP Publishing. 10.1088/1755-1315/988/3/032063
11. Tokarev A, Yanbarisova A, Khatmullina R, editors. The Dependence of the Pump Piping Vibration from the Rotor Speed. IOP Conference Series: Earth and Environmental Science; 2021: IOP Publishing. 10.1088/1755-1315/666/4/042065
12. Javanmardi A, Ibrahim Z, Ghaedi K, Benisi Ghadim H, Hanif MU. State-of-the-art review of metallic dampers: testing, development and implementation. Archives of Computational Methods in Engineering. 2020;27(2):455-78. 10.1007/s11831-019-09329-9
13. Palaev A, Krasnikov A. Ultrasonic Treatment of Welded Joint from External, Internal and Two Sides on Reduction of Residual Welding Stresses. International Journal of Engineering Transactions B: Applications. 2024;37:2171-80. 10.5829/ije.2024.37.11b.04
14. Phu V, Canh T, Lieu P. Optimal parameters of dynamic vibration absorber for linear damped rotary system subjected to harmonic excitation. Vietnam Journal of Mechanics. 2020;42(4):385-400. 10.15625/0866-7136/14897
15. Li H, Yao H, Dou J, Jia R, Wei G. Torsional vibration suppression of cantilever beams system with the PNESI. Journal of Low Frequency Noise, Vibration and Active Control. 2024;43(4):1713-31. 10.1177/14613484241272264
16. Medel-Vera C, Ji T. Seismic protection technology for nuclear power plants: a systematic review. Journal of Nuclear Science and Technology. 2015;52(5):607-32. 10.1080/00223131.2014.980347
17. Wang H, Wang B, Hu L, Luo X. Modeling and Experimental Study on the Influence of Support Stiffness on the Vibration of Piston Pump. Journal of Vibration Engineering & Technologies. 2023;11(7):3069-80. 10.1007/s42417-022-00731-5
18. Shammazov I, Sidorkin D, Dzhemilev E, editors. Research of the dependence of the pipeline ends displacement value when cutting out its defective section on the elastic stresses in the pipe body. IOP Conference Series: Earth and Environmental Science; 2022: IOP Publishing. 10.1088/1755-1315/988/2/022077
19. Xu Z-D, Chen Z-H, Huang X-H, Zhou C-Y, Hu Z-W, Yang Q-H, et al. Recent advances in multi-dimensional vibration mitigation materials and devices. Frontiers in Materials. 2019;6:143. 10.3389/fmats.2019.00143
20. Pshenin VV DE, Rozanova LR, Komarovskii MS. Results of analysis of accident rates of gas distribution systems. Problemy

sbora, podgotovki i transporta nefti i nefteproduktov. 2022;4(138):89-101. 10.17122/ntj-oil-2022-4-89-101

21. Zemenkova MY, Chizhevskaya EL, Zemenkov YD. Intelligent monitoring of the condition of hydrocarbon pipeline transport facilities using neural network technologies. Записки Горного института. 2022;258:933-44. 10.31897/PMI.2022.105
22. Perveitalov OG, Nosov VV, Schipachev AM, Alekhin AI. Thermally Activated Crack Growth and Fracture Toughness Evaluation of Pipeline Steels Using Acoustic Emission. Metals. 2023;13(7):1272. 10.3390/met13071272
23. Shlyannikov V, Tumanov A, Zakharov A, Gerasimenko A. Surface crack growth subject to bending and biaxial tension-compression. Fracture and Structural Integrity. 2016;10(35):114-24. 10.3221/IGF-ESIS.35.14
24. Yusuf M, Latief Y, Rarasati AD, Trigunarsyah B, Laksono NB. Fuzzy Bayesian Belief Networks Method on Risk Assessment of EPC Pipeline Project. Civil Engineering Journal (Iran). 2025;11(3):1050-71. 10.28991/CEJ-2025-011-03-013
25. Baghdasaryan M, Hovhannisyn V. Stability assessment of an ore mill electric drive using machine learning. HighTech and Innovation Journal. 2024;5(2):213-30. https://doi.org/10.28991/HIJ-2024-05-02-01
26. Meena A, Parayil P, Suthar V. Simulation and Validation of FRP Base Plate for Electric Compressor. SAE Technical Paper; 2020. Report No.: 0148-7191.
27. Bolshunov AV, Ignatev SA, Gorelik GD, Krikun NS, Vasilev DA, Rakitin IV, et al. Comprehensive studies of the snow-firn layer in the area of the Russian Antarctic Vostok Station. Journal of Mining Institute. 2025.
28. Shojaee Barjoee S, Rodionov V, Vaziri Sereshk AM. Noise climate assessment in ceramic industries (Iran) using acoustic indices and its control solutions. Advances in Environmental Technology. 2025;11(1):91-115. 10.22104/AET.2024.6922.1899
29. Skamyin A, Shklyarskiy Y, Gurevich I. Influence of background voltage distortion on operation of passive harmonic compensation devices. Energies. 2024;17(6):1342. 10.3390/en17061342
30. Shibanov D, Ivanov S. Failure risks of mine excavator associated with its maintenance and repair. Russian Mining Industry. 2024;2:97-102. 10.30686/1609-9192-2024-2-97-102
31. Khamidov O, Shibanov D, Shishkin P, Kolpakov V. Efficiency of excavators application in open pit mines of Uzbekistan. Min Ind J. 2024;5:135-42. 10.30686/1609-9192-2024-5-135-142
32. Shammazov IA BA, Aleksandruk BS,. Algorithmic Models for Determining the Flow Patterns of Oil Pipelines in Gravity Sections. International Journal of Engineering Transactions A: Basics. 2025;38(10):2476-85. 10.5829/ije.2025.38.10a.22
33. Rousou K, Rani MA, Bahari A, Kyprianou A, editors. Exploratory structural modification and nonlinear based analysis of tuned mass dampers. Journal of Physics: Conference Series; 2024: IOP Publishing. 10.1088/1742-6596/2721/1/012016
34. Cao J, Liu B, Wu Q, Liu J. Research on the vibration control of micro-vibration using a novel hybrid isolator. Experimental Techniques. 2024:1-13. 10.1007/s40799-024-00772-3
35. Zang J, Cao R-Q, Zhang Y-W. Steady-state response of a viscoelastic beam with asymmetric elastic supports coupled to a lever-type nonlinear energy sink. Nonlinear Dynamics. 2021;105(2):1327-41. 10.1007/s11071-021-06625-7
36. Chang Y, Li Y, Zhou J, Wang K, Wang Q, Wen G. Compensation strategy for quasi-zero-stiffness vibration isolator under payload mismatch. Acta Mechanica Sinica. 2024;40(10):524033. 10.1007/s10409-024-24033-x
37. Faraj AK, Hussein HAHA. Application of finite element technique: a review study. Iraqi Journal of Chemical and Petroleum Engineering. 2023;24(1):113-24. https://doi.org/10.31699/IJCPE.2023.1.13
38. Fedorova E, Morgunov V, Pupysheva E. Effect of variation of internal diameter along the length of a rotary kiln on material movement. Non-ferrous Metals. 2024;56(1):28-34. 10.17580/nfm.2024.01.05
39. Chigarev A, Kravchuk A, Smalyuk A. ANSYS for engineers: reference manual. Mechanical Engineering. 2004;1.
40. Wang Z, Zhang Q, Zhang K, Hu G. Tunable digital metamaterial for broadband vibration isolation at low frequency. Advanced materials. 2016;28(44):9857-61. 10.1002/adma.201604009
41. Almashhor A, Asiri SA. Development of a new tuned vibration absorber based on one degree-of-freedom of translational motion. Cogent Engineering. 2021;8(1):1976929. 10.1080/23311916.2021.1976929
42. Pshenin V, Menshikov S, Komarovskiy M, editors. Study of static charge accumulation in HDPE gas pipelines. E3S Web of Conferences; 2023: EDP Sciences. 10.1051/e3sconf/202337802001
43. Schipachev A, Fetisov V, Nazyrov A, Donghee L, Khamrakulov A. Study of the pipeline in emergency operation and assessing the magnitude of the gas leak. Energies. 2022;15(14):5294. 10.3390/en15145294

Persian Abstract

چکیده

اهمیت این تحقیق ناشی از ضرورت ارتقای سیستم‌های جبران ارتعاش موجود برای کاهش بارهای ارتعاشی بر روی واحدهای قدرت واحدهای پمپاژ خط اصلی (MPU) است. الگوریتم‌ها و نتایج محاسباتی وضعیت ارتعاش فضایی سیستم جبران ارتعاش (VCS) برای MPUها تحت رژیم‌های عملیاتی مختلف ارائه شده است. مدل‌های ریاضی و فضایی المان محدود، و همچنین نمونه‌های اولیه دیجیتال همه‌کاره VCS، توسعه داده شده‌اند. نوآوری یافته‌ها در نمونه اولیه دیجیتال توسعه‌یافته MPU نهفته است که قابلیت‌های گسترده‌ای را برای در نظر گرفتن عوامل طراحی-فنی ارائه می‌دهد، رژیم‌های عملیاتی متنوع را در خود جای می‌دهد و دقت و کارایی محاسباتی بالایی را نشان می‌دهد. اهمیت عملی این کار این است که روش شبیه‌سازی توسعه‌یافته مبتنی بر نمونه‌های اولیه دیجیتال MPU VCS، تجزیه و تحلیل اثرات ارتعاشی موتورهای الکتریکی، پمپ‌ها و قاب‌های تحمل بار را امکان‌پذیر می‌سازد. مطالعات محاسباتی جامعی در مورد وضعیت تنش-کرنش قاب VCS انجام شد و فرکانس‌های طبیعی سیستم در حین کار ارزیابی شدند. هدف از این کار، مطالعه رفتار واحد پمپاژ هنگام جایگزینی تکیه‌گاه‌های الاستومری در سیستم جبران با میراگرهای هیدروفیلمی است. یکی از مزایای غیرقابل انکار مدل دیجیتال توسعه‌یافته، پایه و اساس آن برای یک روش‌شناسی جهانی برای ارزیابی اثربخشی جبران‌کننده‌های ارتعاش در MPU VCS است. یک نمونه اولیه دیجیتال منحصر به فرد از MPU با در نظر گرفتن VCS مهندسی‌شده توسعه داده شد. امکان‌سنجی استفاده از یک نمونه اولیه دیجیتال مبتنی بر المان محدود برای ارزیابی بارگذاری ارتعاشی روی MPUها اثبات شده است. آزمایش‌های عددی با استفاده از دوقلوی دیجیتال MPU نشان داد که پیاده‌سازی میراگرهای هیدروفیلمی در VCS، تنش‌های دینامیکی اوج را ۱۸٪ کاهش می‌دهد. مقادیر جابجایی‌های محوری و منتج MPU با استفاده از میراگرهای هیدروفیلمی و الاستومری در VCS به ترتیب ۱۱/۱ میلی‌متر و ۱۰/۰ میلی‌متر اندازه‌گیری شدند.